Eletrônica de Potência
Open Journal of Power Electronics

Received April 24, 2024; accepted July 04, 2024; Date of publication August 07, 2024.
The review of this paper was arranged by Associate Editor Roberto F. Coelho and Editor-in-Chief Heverton A. Pereira.

Digital Object Identifier http://doi.org/10.18618/REP.2005.2.023027

Optimized Design Methodology and Maximum Efficiency Tracking Algorithm for Static IPT Chargers in Electric Vehicles

Leonardo A. Brum Viera [1], Pedro Pascoal [2], Cassiano Rech [1]

[1]Federal University of Santa Maria, Department of Electrical Energy Processing, Santa Maria - RS, Brazil
[2]Institute of Systems and Computer Engineering, Technology and Science, Porto, Portugal

e-mail: leonardo.viera@ufsm.acad.br, pedro.pascoal@inesctec.pt, cassiano.rech@ufsm.br.

ABSTRACT In recent years, technologies related to the electrification of transportation have attracted significant attention. Among these, wireless charging stands out, even facing numerous challenges concerning design and parameter optimization. Consequently, this article introduces a novel design methodology to improve the performance of inductive power transfer (IPT) systems for wireless charging applications in electric vehicles. The methodology considers operational limits of switches and passive components. By using a combination of Newton-Raphson and Particle Swarm Optimization (PSO) algorithms, the proposed approach efficiently determines both electrical and physical parameters of converters and coils to achieve maximum efficiency at a chosen operational point. Furthermore, a Maximum Efficiency Point Tracking (MEPT) algorithm is employed for optimal system operation. The proposed methodology is validated through experimental analysis using a 3.6 kW setup. Results demonstrate a power transfer efficiency around 89.4 %, while ensuring that current and voltage levels remain within safe operating areas for the components.

KEYWORDS Electric Vehicle, Inductive Power Transfer (IPT), Optimization Design, Particle Swarm Optimization (PSO), Wireless Charger, Wireless Power Transfer (WPT).

I. INTRODUCTION

The increasing adoption of electric vehicles (EVs) is a sustainable solution for urban mobility. Data from the International Energy Agency (IEA) demonstrates a significant growth in the EV fleet and a doubling of sales in 2021, driven by various factors such as political support, commitments to phase out internal combustion engines, and initiatives from automakers to electrify their fleets [1].

In addition, the rise in EV adoption in Brazil reflects the growing interest in sustainable mobility, aligning the country with this global trend. With more countries and regions prioritizing the transition to electric vehicles, continued growth in the EV market and a reduction in the environmental impact of transportation are expected [2]. However, adoption of EVs face some barriers like low energy density and high cost of batteries, resulting in limited autonomy compared to combustion vehicles. Improving battery technology and charging infrastructure is crucial for addressing these challenges in urban electric transportation.

One innovative technology in this field is the Wireless Power Transfer (WPT) charging system. The WPT enables convenient and efficient charging of EVs without the need for physical cables, offering greater convenience and accessibility for EV owners. Inductive Power Transfer (IPT), one of the WPT technologies, is extensively used in electric vehicle charging applications [3]–[5]. It's greatest advantages compared to other WPT techniques is the superior performance for operation at medium distances, smaller volume of transceivers, and better performance for high power levels, which aligns with the requirements stipulated in standards [6]–[9].

When designing IPT systems one of the main concerns is about PTE (Power Transfer Efficiency). Various methodologies can be employed to maximize its efficiency, even considering load variations and misalignment operations. An optimization technique is presented in [10], using multiple transmitting coils and adaptive control to select the coil most aligned with the vehicle to maximize PTE. In [11], a 2-D finite-element analysis (FEA) to determine the optimum design parameters of the system coils is presented, comparing misalignment and coils cost. In all these techniques, the design starts with the geometry of the coils and then the components are chosen based on the magnitudes of the electrical variables. However, it would be important to design the IPT system taking into account the current and voltage limits imposed to the circuit to suit the available components.

In addition to the optimized design, it is essential to ensure that the system remains at a point of maximum efficiency, where switching and conduction losses are minimized for the same transferred power. Furthermore, the IPT charger

should exhibit robustness against disturbances such as coil misalignment and load variation. In the literature, complex MEPT (Maximum Efficiency Point Tracking) techniques are found [12], where analytical equations are used to estimate the dynamic coupling factor, consequently allowing for the determination of the optimized point. In [13], a machine learning-based algorithm is employed to accurately estimate efficiency throughout the operation, considering misalignment variations. While the algorithm demonstrates precision, a downside is the amount of data required to train it, as well as its lack of generalization to all applications. In this work, the algorithm proposed in [14] and [15] is utilized, which has been experimentally validated only for low-power applications.

Therefore, this article proposes a new approach to increase the efficiency of IPT system through the optimization of design variables using the PSO algorithm, assuming maximum voltage and current boundary conditions in the components. This article is an expanded version of [7], including a detailed analysis of the equations that govern the physical parameters of the coils, in addition to new results obtained and a discussion of an efficiency tracking algorithm used during the operation of the converter.

This article is organized as follows: the operational principles of the IPT system are discussed in Section II, and a comprehensive presentation of the proposed design methodology is presented in Section III. Experimental results are included in Section IV to validate the effectiveness of the optimization technique in achieving maximum system efficiency.

II. DESCRIPTION OF THE IPT SYSTEM

The IPT system under study is illustrated in Figure 1. The circuit has two main parts: one external to the vehicle (transmission side) and other embedded in the vehicle (receiving side).

The transmission side is composed by a high-frequency DC-AC full-bridge inverter, a transmission coil, represented by the inductance L_1 and the compensation capacitance (C_1). The inverter has the function of injecting high-frequency alternating current into the transmission coil, which in turn generates an electromagnetic field. Due to the high-reluctance air core, it is necessary to insert the compensation circuit, in this case, a capacitor in series, sized to compensate the leakage inductance of the primary coil. In addition, the IPT charger has a front-end converter (usually a PFC boost converter) connected to the grid, but it is not the main focus of this work. Therefore, it was not considered in this analysis.

The receiving side comprises a receiving coil,represented by the inductance L_2, the compensation capacitor (C_2), a passive ac-dc full-bridge rectifier and a synchronous buck-boost converter. In this part of the circuit, the receiving coil captures the electromagnetic field produced by the primary coil, which is compensated by the series capacitor and then rectified by the full-bridge diode rectifier, generating an intermediate dc bus voltage for the buck-boost converter connected to the EV battery bank.

The system is controlled in the primary and secondary sides, where the secondary buck-boost converter has the function of guaranteeing adequate voltage and current levels for battery charging, while the primary inverter uses a perturb and observe algorithm to track the maximum efficiency transmission point.

A. SERIES-SERIES STEADY-STATE ELECTRICAL MODEL

The design methodology relies on the steady-state analytical equations of the circuit. Consequently, a simplified circuit is considered for modeling. For this purpose, a first harmonic approximation is utilized, which considers that in a resonant system the only component of the Fourier series contributing to power transfer is the fundamental frequency component [16]. Through this approximation, it is possible to replace the input inverter by an ac voltage source at the resonance frequency of the system. Furthermore, the battery, output rectifier and buck-boost converter can be replaced by an equivalent resistive load, representing a specific operation point. The resulting simplified circuit is illustrated in Figure 2, where r_{L1}, r_{L2}, and R_{oe} represent, respectively, the resistance of the transmission coil, the resistance of the reception coil, and the equivalent load resistance of the circuit. The voltage v_{ie} represents the amplitude of the first harmonic component synthesized by the inverter, considering symmetric phase-shift modulation. The relationship between the modulation angle (φ) and v_{ie} can be expressed as follows [17]:

$$v_{ie} = \frac{1}{2\sin^{-1}\left(\frac{\pi\sqrt{2}}{4\varphi V_{in}}\right)}. \tag{1}$$

The equivalent output resistance (R_{oe}) can be found using the static gain of the buck-boost converter, where the resistance reflected at the converter input (R_{eq}) is expressed by [18]:

$$R_{eq} = \left(\frac{1-D}{D}\right)^2 R_o \tag{2}$$

where R_o represents the equivalent resistance of the battery determined using power and voltage measurements at a specific operating point, and D is the duty-cycle of buck-boost converter. Considering the Fundamental Harmonic approximation (FHA) [19], the equivalent R_{oe} could be expressed as:

$$R_{oe} = \frac{8}{\pi^2} R_{eq}. \tag{3}$$

In compensation topologies, IPT can be designed in two ways. The first involves designing the capacitors to operate in resonance with the leakage inductances, while in the second method, capacitors are sized for resonance with the self-inductances of the coils. In [20], both techniques are compared, with self-inductance compensation presenting higher efficiency and greater robustness against coil misalignment variations. Therefore, one can choose to perform this analysis

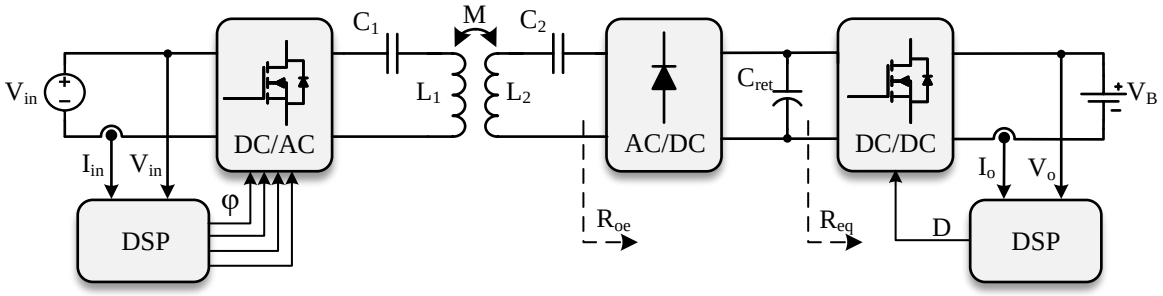

Figure 1. IPT electric charging system.

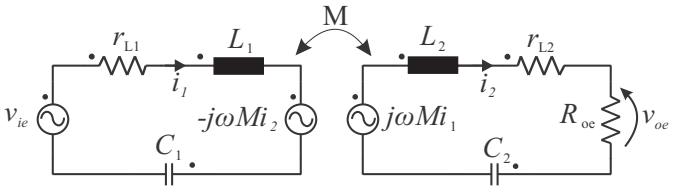

Figure 2. IPT simplified circuit.

considering capacitors C_1 and C_2 operating in resonance with self-inductances L_1 and L_2, respectively. Thus, the capacitances of the circuit can be desinged from:

$$C_1 = \frac{1}{\omega^2 L_1}, \qquad C_2 = \frac{1}{\omega^2 L_2}. \tag{4}$$

In this way, for an operating frequency ω_0 the primary and secondary reactances are cancelled, so that:

$$1/j\omega_0 C_1 = j\omega_0 L_1, \qquad 1/j\omega_0 C_2 = j\omega_0 L_2. \tag{5}$$

For the static analysis, the dynamic voltage and current components were replaced by their steady-state phasor equivalents. The phasors are the rms values of the sinusoidal voltages and currents, defined by:

$$\begin{aligned} v_{ie} &= V_{ie}\sqrt{2}\sin(\omega t), \\ i_1 &= I_1\sqrt{2}\sin(\omega t + \theta_1), \\ v_o &= V_o\sqrt{2}\sin(\omega t + \theta_2), \\ i_2 &= I_2\sqrt{2}\sin(\omega t + \theta_2). \end{aligned} \tag{6}$$

Using Kirchhoff Law it is possible to write the primary current (I_1) and secondary current (I_2) as:

$$I_1 = \frac{V_{ie}(r_{L2} + R_{oe})}{\omega^2 M^2 + r_{L1}(r_{L2} + R_{oe})}, \tag{7}$$

$$I_2 = \frac{V_{ie}(j\omega M)}{\omega^2 M^2 + r_{L1} r_{L2} + R_{oe} r_{L1}}. \tag{8}$$

Multiplying (8) by the load resistance R_{oe} one can obtain the output voltage, represented by

$$V_o = \frac{V_{ie}(j\omega M) R_{oe}}{\omega^2 M^2 + r_{L1} r_{L2} + R_{oe} r_{L1}}. \tag{9}$$

Multiplying (8) and (9) gives the following expression for output power:

$$P_o = \frac{{V_{ie}}^2 \omega^2 M^2 R_{oe}}{\left[\omega^2 M^2 + r_{L1} r_{L2} + R_{oe} r_{L1}\right]^2}. \tag{10}$$

The apparent input power is calculated by multiplying the rms value of the input voltage V_{ie} by (7), and it can be expressed as:

$$S_{in} = \frac{{V_{ie}}^2 (r_{L2} + R_{oe})}{\omega^2 M^2 + r_{L1}(r_{L2} + R_{oe})}. \tag{11}$$

The input active power can be calculated by multiplying (11) and the cosine of the phase difference between v_{ie} and I_1. However, it is observed that (7) does not have an imaginary part due to the compensation method used. Where, as seen in the equation 5 for operation with a switching frequency equal to the resonant frequency, the capacitor fully compensates the coils' self inductance. In this way, the system does not present a phase difference between the input current and voltage, operating with unity power factor. Therefore, the input power can be given as:

$$P_{in} = \frac{{V_{ie}}^2 (r_{L2} + R_{oe})}{\omega^2 M^2 + r_{L1}(r_{L2} + R_{oe})}. \tag{12}$$

Therefore, the circuit efficiency can be obtained from (10) and (12), and it can be given by:

$$\eta = \frac{R_{oe}}{\left[1 + \frac{r_{L1}(r_{L2} + R_{oe})}{\omega^2 M^2}\right](r_{L1} + r_{L2})}. \tag{13}$$

The voltage across the capacitors can be calculated from:

$$V_{C1} = \frac{I_1}{j\omega_0 C_1}, \qquad V_{C2} = \frac{I_2}{j\omega_0 C_2}. \tag{14}$$

B. COILS DESIGN

The electromagnetic coupling of a IPT system is composed of two coils. The main parameters under consideration during the design of these coils are the coupling coefficient and the quality factor [21]. The first is predominantly influenced by the spacing between the coils and their misalignment. Consequently, to achieve the target coupling coefficient, the

coil must be designed for a specific distance and misalignment values. The latter is enhanced through the reduction of conductor resistance (r_L), which depends on the skin effect, proximity effect, and dispersion losses, and by amplifying the values of self-inductance [22].

Currently, the literature presents various coil configurations, including circular, square, rectangular, and three-dimensional spiral (solenoid). These designs serve as foundational models for the development of other arrangements, such as the DD coil, DDQ, and bipolar multi-coils [22].

In the studies conducted in [23] and [24], it was deduced that the circular coil occupies less space, requires a smaller amount of material, and exhibits greater tolerance to misalignment. This culminates in enhanced performance concerning mutual inductance parameters, coupling coefficient, magnetic flux, and magnetic field. In this context, the circular coil is esteemed as an exemplary choice in IPT systems, and the design variables are illustrated in Figure 3. Parameters D_o and D_i are, respectively, the external and

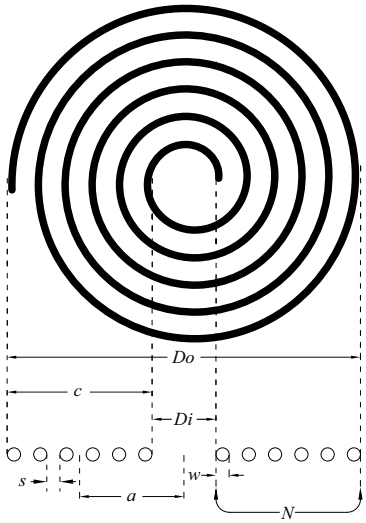

Figure 3. Parameters of the flat circular coil.

internal diameters of the coil. The section of the conducting wire is represented by w, the spacing between the turns is described as s, and N symbolizes the number of turns.

The self-inductance of the coils is a crucial requirement for the IPT system, determining the resonance, also, it contributes to enhancing the quality factor and, alongside mutual inductance, establishes the prescribed coupling coefficient. The self-inductance of flat circular coils is estimated by:

$$L_x = 31,33\mu_0 N^2 \left(\frac{a^2}{(8a)+(11c)}\right)\mu H \tag{15}$$

where subscript x is the primary and secondary coils (given in micro-Henry), and the variables a and c are given by

$$a = \frac{(D_o + D_i)}{4}, \tag{16}$$

$$c = \frac{(D_o - D_i)}{2} \tag{17}$$

and μ_0 represents the permeability of the vacuum, given by:

$$\mu_0 = 4\pi.10^{-7}\ H/m. \tag{18}$$

Note that to determine the self-inductance, their internal diameter is necessary, which can be established according to:

$$D_i = D_o - (2wN) - (2s(N-1)). \tag{19}$$

To determine the mutual inductance between the coils, numerical methods are usually implemented, such as the Boundary Element Method (BEM) and the Finite Element Method (FEM). However, mutual inductance can be obtained based on the concepts of the Biot-Savart and Faraday-Lenz laws, analytically, as follows:

$$M = -\frac{\rho_1\mu_0 N_1 N_2}{4\pi}\int_{\rho_2=0}^{\rho_2}\int_{\phi_2=0}^{2\pi}\int_{\phi_1=0}^{2\pi}\frac{\rho_2(A\cos\phi_1 + B\sin\phi_1)}{r^3}d\phi_1 d\phi_2 d\rho_2 \tag{20}$$

where:

$$\begin{cases}\rho_1 = \text{a = Radius of primary coil (m)}\\ \rho_2 = \text{Radius of secondary coil (m)}\\ \text{A} = \rho_2\cos\phi_2 - \text{a}\cos\phi_1\\ \text{B} = \rho_2\sin\phi_2 - \text{a}\sin\phi_1\\ \text{r} = \sqrt{\rho_2^2 + \text{a}^2 - 2\rho_2\text{a}\cos(\phi_2-\phi_1) + \text{D}^2}\\ \text{D} = \text{Distance between coils (m).}\end{cases}$$

Equations (15) - (19) were derived from the results reported in [25], while (20) was deduced. All these equations were subsequently validated through finite element simulation, as demonstrated in [26].

Based on the mutual inductance and the self-inductance of the coils, it is possible to estimate the coupling factor, such as a function of the distance between the coils, as expressed by the following equation:

$$k = \frac{M}{\sqrt{L_1 L_2}}. \tag{21}$$

Another important variable for the methodology proposed in the article is the resistance of the coils, which is used to estimate the efficiency of the system. In this design methodology is proposed to use litz wire to build the coils, as recommended in the standard [27], therefore the resistance can be estimated by:

$$R_w = \frac{\rho l}{A_{str}.N_{str}}.k_{nb}.k_{BW} \tag{22}$$

R_w represents the total resistance of the conductor since ac losses are ideally eliminated using the Litz wire. ρ and l are the resistivity of the copper and the conductor length, respectively. N_{str} corresponds to the total number of conductors (*strands*) making up the Litz wire, and A_{str} symbolizes the area of each of these conductors. The variables k_{nb} and k_{BW} are related to the yarn length shortening factor due to the strand bundling process and factor of possible broken wires, respectively.

III. DESIGN OPTIMIZATION TECHNIQUE

A. DESIGN SPECIFICATIONS

Table I shows the specifications of the IPT charger under development.

Table 1. Design specifications for the IPT system

Parameter	Sym	Value
Input Voltage	V_{in}	400 V
Output Nominal Voltage	V_o	360 V
Nominal Output Power	P_o	3.6 kW
Operation Frequency	f_s	85 kHz
Coils Gap	D_{Gap}	160 mm
Nominal coupling factor	k	0.2
Compensation topology		Series-Series

The operating frequency and the distance between the coils are defined based on the SAE-J2954 standard [28]. The operating frequency can vary between 79 kHz - 90 kHz. The definition of the distance between the coils is based on the Z2 class, which defines nominal operation for a distance between 100 mm and 210 mm.

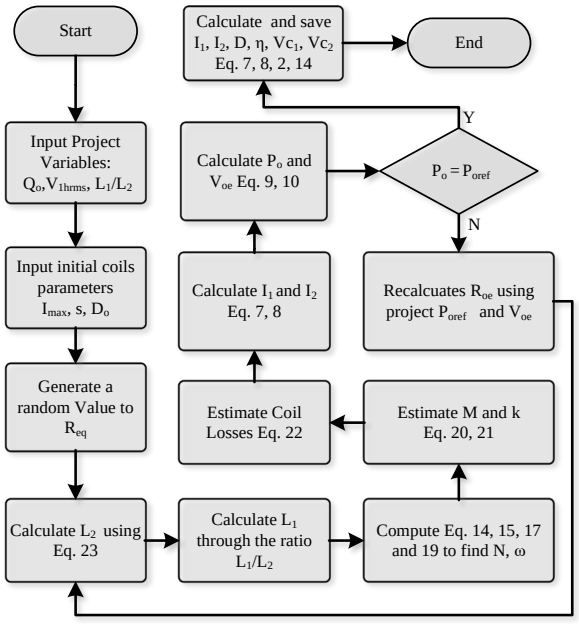

Figure 4. Flowchart diagram of the interactive algorithm for IPT circuit simulation.

B. ITERATIVE IPT SIMULATION ALGORITHM

The proposed design methodology uses a simplified model of the system, as shown in Figure 2. Analyzing this figure, the circuit has four main variables that can be used to interact with the algorithm: ac input voltage amplitude (V_{ie}), t he inductance L_1, the inductance L_2 and the duty cycle of the buck-boost converter (D) intrinsic to the R_{oe}. The other parameters such as series resistance of the coils (r_{L1} and r_{L2}) and compensation capacitors (C_1 and C_2) are linked to the inductance values and the physical design of the coils.

In the design of resonant converters, the output quality factor (Q_o) is a variable typically used as a design parameter. This factor generally ranges between 2 and 10 for IPT systems, as a higher value can make the system difficult to tune, and a lower value will generate harmonics in the current and voltage waveforms [29], [30] and can be defined as:

$$Q_o = \frac{\omega_0 L_2}{R_{oe}} \tag{23}$$

where ω_0 is the operating frequency, in rad/s.

From (23), one can observe that the quality factor is dependent on both the output load resistance and the self-inductance of the secondary coil. Consequently, new design variables can be defined: the input voltage (V_{ie}), and the output quality factor (Q_o), which incorporates the duty ratio and secondary self-inductance. Additionally, a ratio between the primary and secondary inductance's (L_1/L_2) can be defined as a variable instead of directly assigning an arbitrary value for L_1.

The boundaries of the algorithm are divided into electrical and geometrical constraints. Electrical constraints encompass maximum currents in coils, maximum voltages across capacitors, maximum inverter-synthesized voltage, and the duty cycle range of the buck-boost converter. Geometrical constraints relate to the physical implementation of the coils, specifically limiting the number of turns based on the inner radius. Predefined parameters include the outer radius and conductor spacing, with the algorithm adjusting the number of turns to achieve the desired inductance.

Based on these three design parameters, an iterative algorithm has been developed, based on the flowchart given in Figure 4, aiming to simulate the behavior of the main circuit variables by varying the design parameters. In this case, it was decided to check the behavior of the primary rms current I_{1rms}, secondary rms current I_{2rms}, peak voltage in the capacitors V_{C1pk} and V_{C2pk}, the duty ratio of the buck-boost converter (D) and the circuit efficiency (η). The Newton Raphson algorithm was used to compute the variables of the system, the variables converge to the values that guarantee the power and output voltage specified in the project. As an example, the variables of interest are shown in Figure 5 as a function of the quality factor that varies between (0 - 10), the input voltage that varies between (100 V - 400 V), maintaining the ratio (L_1/L_2) constant and equal to 0.89.

This example does not encompass the optimization process; rather, Figure 5 illustrates the planes that define the behavior of the variables of interest (including efficiency) in relation to the design variables. These represent all possible design options, essentially the planes where the algorithm will find the optimal point.

All points belonging to the three-dimensional planes illustrated in Figure 5 satisfy the design specifications. However, depending on the operating point it is possible to obtain specific characteristics for the variables of interest (D, I_1, I_2,

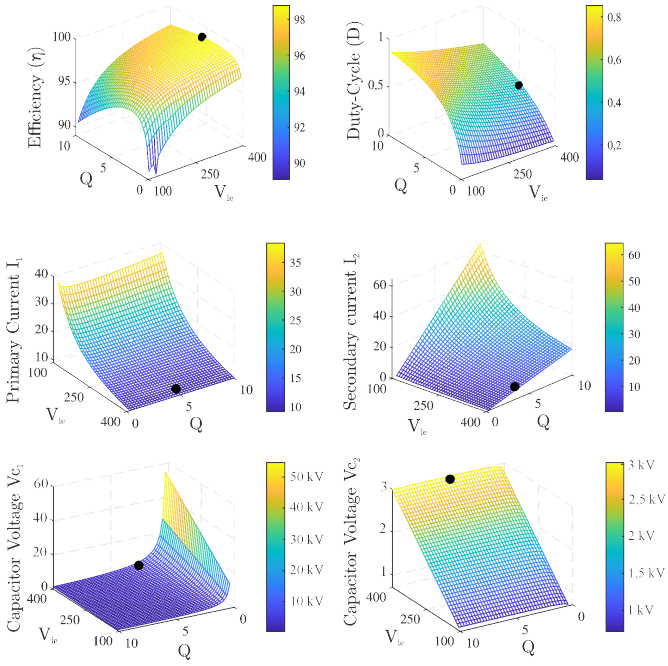

Figure 5. Analysis of the simplified model: (a) η , (b) D , (c) I_1 , (d) I_2 , (e) V_{C1} and (f) V_{C2} as a function of the variation of Q_o and V_{ie} keeping the ratio L_1/L_2 fixed at 0.89.

V_{C1} and V_{C2}). As an example, the black dot positioned in the graphs was chosen for obtaining maximum circuit efficiency. It can be seen that at this point the peak voltage in the capacitors reaches high values, which could be a problem with regard to the insulation of the circuit components. Furthermore, this voltage level is also reflected at the terminals of the transmission and reception coils, thus complicating their physical design. Therefore, it becomes interesting to develop a design method that guarantees maximum efficiency taking into account some operational restrictions.

C. OPTIMIZATION DESIGN ALGORITHM

The objective of the optimization algorithm is to adjust the design variables to meet the design specifications while maximizing efficiency. This involves maximizing the quality factor of the coils while seeking operation with lower current magnitudes for the same transferred power. Thus, semiconductor conduction losses will also be minimized. Additionally, the algorithm must ensure operation within maximum limits based on available components. This leads to the formulation of an optimization problem, presented as:

$$\begin{aligned} &\max \Im \rightarrow Eq.(13). \\ &\text{subject to g} \rightarrow \left\{ \begin{array}{c} V_{C1} < V_{C1_{pk}} \\ V_{C2} < V_{C2_{pk}} \\ I_1 < I_{1_{ref}} \\ I_2 < I_{2_{ref}} \\ D_{\min} < D < D_{\max} \end{array} \right\}. \end{aligned} \tag{24}$$

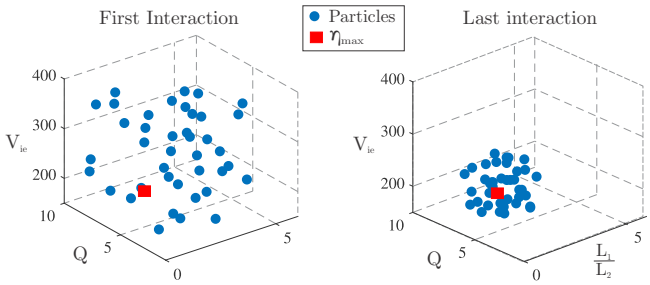

Figure 6. Position of particles in the plane (V_{ie}, L_1/L_2, Q). (a) First iteration. (b) Last iteration.

In this optimization problem, the objective is to maximize the cost function $\Im$, while subjected to the constraints outlined in g. The selected optimization approach for parameter design is Particle Swarm Optimization (PSO), a population-based algorithm inspired by the collective behaviors observed in bird flocks or fish schools. PSO iteratively enhances a population of potential solutions by adjusting their positions in the search space based on both individual experiences and those of their neighbors. This iterative process aims to converge towards the optimal solution for the specified problem.

The PSO was chosen for its ease of implementation, requiring minimal parameter tuning, and robust precision. However, even a brute force algorithm could yield similar results, though with a significant computational cost due to high-resolution requirements, particularly when optimizing with three or more variables. Moreover, extending optimization to the physical design of coils introduces at least 3 additional variables. Hence, PSO emerges as an adequate tool for scaling problems with a multitude of variables [31].

The solutions in the PSO algorithm are called particles, which travel through an n-dimensional space formed by the parameters to be varied. The particles move using the best positions found as a reference, where the best position is the one in which the objective function reaches the maximum/minimum values. The algorithm has been executed using the design specifications and the following operating limits: $I_{1ref} \leq 20$ A, $I_{2ref} \leq 20$ A, $V_{C1} \leq 1600$ V_{pk}, $V_{C2} \leq 1600$ V_{pk}, $V_{ie} \leq 400$ V, $0.3 < \text{D} < 0.70$, D_o = 50 cm.

Figure 6 illustrates the behavior of the particles for the first and last iteration of the algorithm, where the red square represents the position of the particle whose highest efficiency was obtained, respecting the established limits. It can be observed that throughout the interactions the particles concentrate around a zone that the algorithm interprets as having the best solutions to the problem. Table 2 presents the design parameters found for the arbitrated specifications and restrictions.

Table 2. Resulting design parameters.

Parameter	Sym	Value
Primary inductance of the coil	L_1	120 μH
Secondary inductance of the coil	L_2	136 μH
Input voltage	V_{ie}	210 V
Duty-Cycle of Buck-Boost converter	D	0.577
Compensation capacitor	C_1	29.11 nF
Secondary compensation capacitor	C_2	25.71 nF
Series resistance primary inductor	r_{L1}	128 mΩ
Series resistance secondary inductor	r_{L2}	137 mΩ
Output resistance	R_{oe}	15.68 Ω

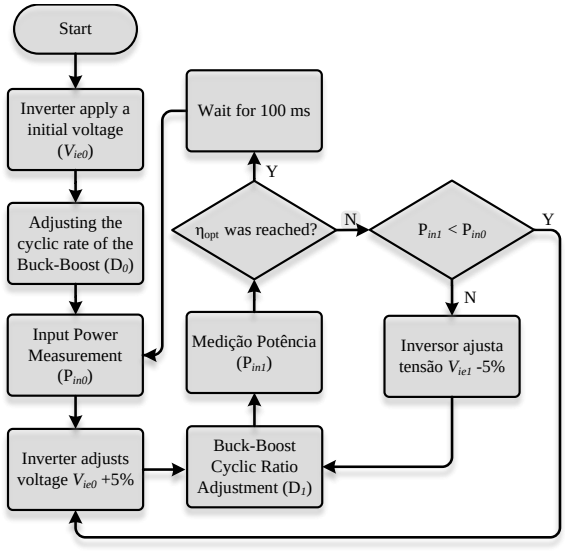

Figure 7. Flowchart of MEPT algorithm.

IV. MAXIMUM EFFICIENCY POINT TRACKING (MEPT) ALGORITHM

This section aims to present the algorithm responsible for controlling the inverter, ensuring system operation under conditions of maximum efficiency under load variations and misalignment. Control strategies for IPT systems can be classified by: primary control, secondary control or or dual-side control. The proposed control is a dual-side strategy [15], [14], as illustrated in Figure 1.

In this control strategy, output current and voltage are used for controlling the buck-boost converter, which main function is to control the battery charging. This is achieved through the implementation of a dual-loop voltage and current control scheme. Input current and voltage are employed for inverter control, using a maximum efficiency tracking algorithm, as depicted in Figure 7.

The main concept is to guarantee constant power at the output and modify the control action of the input inverter to demand the lowest power from the energy source.

The inverter modulation is based on the phase-shift technique, known as SVC (Symmetrical Voltage Cancellation) [17]. The output of MEPT algorithm (in %) is converted to an RMS voltage and applied to (1), which determines the phase angle for generating the PWM signal, ranging from 0º to 180º. The switching frequency is maintained constant, due to small switching frequency range imposed by SAE J2954 [9], thereby restricting the flexibility of the controller.

Table 3. Parameters of the implemented coils.

Parameters	Tx Coil	Rx Coil	Unit
Inductance (L)	120	135	μH
Number of turns (N)	12.5	13.5	-
Inner diameter (D_i)	375	365	mm
Outer diameter (D_o)	500	500	mm
Wire length (l)	19	20	m
Equivalent resistance (R_w)	84.8	52.3	mΩ
Mutual inductance (M)	23.76	27.09	μH
Coupling coefficient (k)	0.202	0.202	-

V. EXPERIMENTAL VALIDATION

This section presents some experimental results obtained through the development of a prototype to validate the IPT converter design for applications in EV chargers. Figure 8 shows a picture of the experimental setup. It can be seen that the coils are installed on a platform that allows vertical and horizontal distance adjustment. For nominal system operation, the vertical distance is 16 cm and the horizontal misalignment can vary up to 22 cm. Another feature of the coil platform is that its structure is entirely built with non-ferromagnetic materials, which contributes to more accurate measurements, where the induction of eddy currents can be minimized. The practical parameters of the coils are given in Table 3.

The primary goal of the initial analysis is to ensure that operational limits are not exceeded, based on the nominal operating point. Therefore, Figure 9 shows the voltages across capacitors and currents through coils. Notably, the analysis reveals that the maximum peak voltage in the compensation capacitors remains within the specified design limits, as well as for primary and secondary currents.

In addition, Figure 10 presents the voltage synthesized by the high-frequency inverter and the primary current. Firstly, examining the voltage synthesized by the inverter and the current in the primary tank, one can observe that they are nearly in phase. This observation leads to the conclusion that the resonant circuit is fully compensated, implying that only active power is drawn from the source. Consequently, this results in a reduction of conduction losses. Additionally, through the phase-shift modulation technique, ZVS (Zero Voltage Switching) is achieved in two of the four inverter switches, as depicted in Figure 10. This achievement significantly contributes to an overall reduction of the circuit losses.

Figure 11 illustrates an estimation of the distribution of losses across various components of the system. Notably, the semiconductor devices in the input inverter and the output

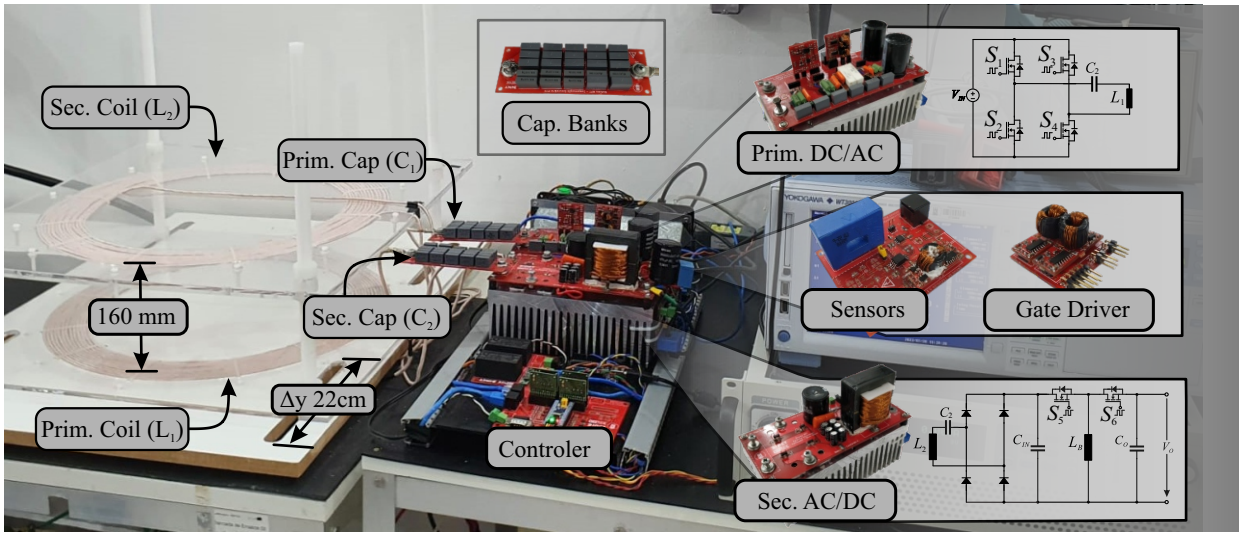

Figure 8. IPT charging prototype.

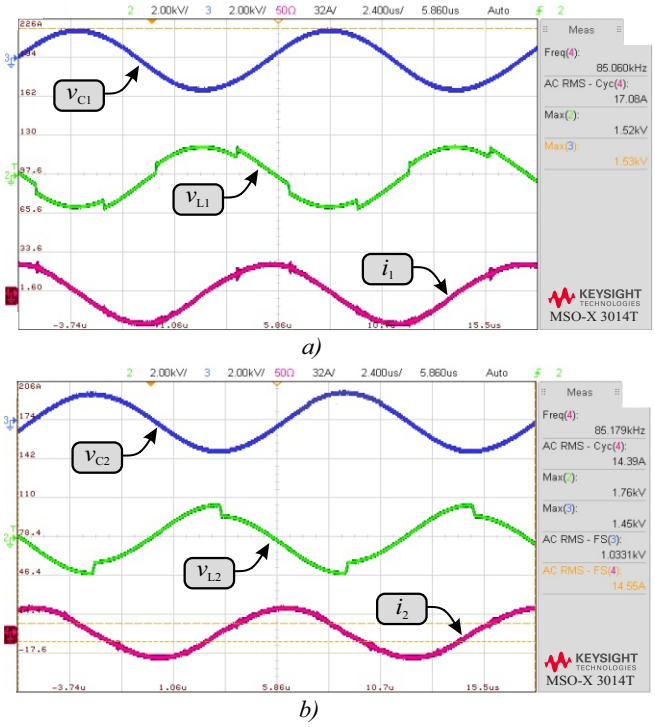

Figure 9. a) Voltage in the primary capacitor (v_{C1}), voltage in the primary coil (v_{L1}) and primary current (i_1). b) Voltage in the secondary capacitor (v_{C2}), voltage in the secondary coil (v_{L2}) and secondary current (i_2).

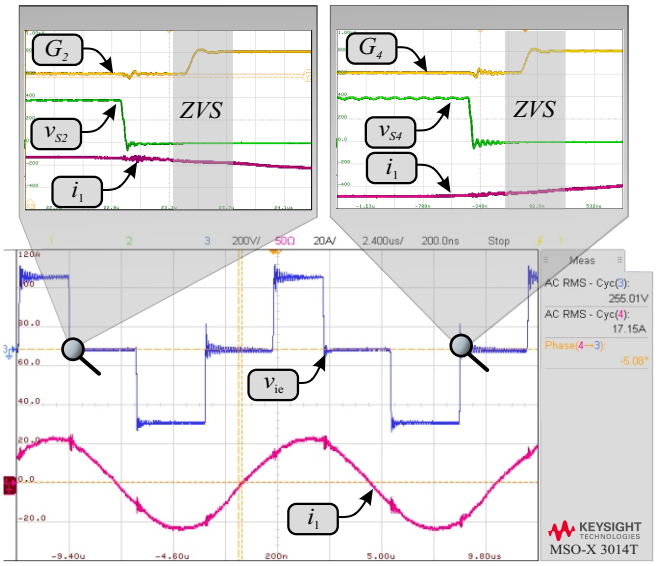

Figure 10. Voltage waveform synthesized by the inverter (v_{ie}), gate signals for low side switches S_2 and S_4 (G_2 and G_4) , voltages across the switches (v_{S2} and v_{S4}) and primary current (i_1).

buck-boost converter account for the largest share of losses, with coils contributing approximately 19 % to the total system losses.

An efficiency analysis was carried out with the Yokogawa WT3000E analyzer, where a total efficiency of 89.4 % was obtained for nominal operation from dc input to dc output.

Figure 12 illustrates the efficiency of the IPT converter by varying the output power, comparing the performance with constant inverter modulation to that with activation of the maximum efficiency algorithm.

One can observe that for low output power levels, the efficiency significantly improves with the implementation of the MEPT algorithm. This improvement occurs because the magnitude of the secondary current in the resonant tank depends solely on the voltage synthesized by the inverter, regardless of the load. Consequently, maintaining the inverter at nominal modulation ensures the same secondary current for both 500 W and 3600 W outputs. Therefore, the conduc-

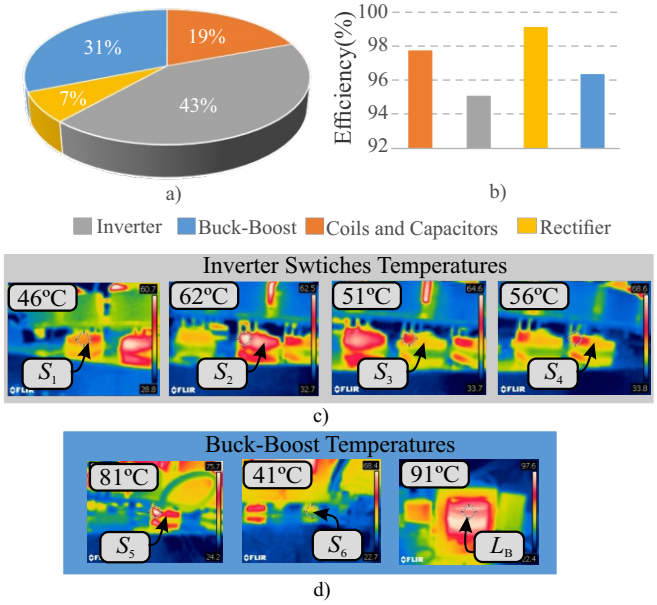

Figure 11. Loss estimation and temperatures of the IPT system: a) Distribution among the components, b) Individual efficiency of each stage, c) Case temperatures of inverter switches, d) Case temperatures of switches and inductor of buck-boost converter.

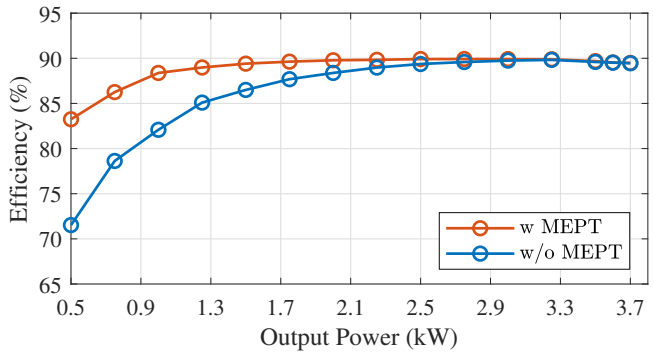

Figure 12. System efficiency varying the output power, with or without MEPT.

tion losses in the secondary components remain constant, leading to a considerable reduction in system efficiency for low power levels. This issue is mitigated by adjusting the inverter modulation.

Considering practical scenarios where a driver might park an electric vehicle misaligned with the charger. Figure 13 depicts IPT system efficiency considering misalignment from 0 to 10 cm, both with and without tracking, while operating at a fixed output power of 3 kW. The reduction in system efficiency resulting from misalignment stems from a decrease in the coupling factor, consequently leading to an increased primary current. Nonetheless, this adverse impact can be mitigated by adjusting the inverter modulation, as demonstrated in Figure 13. Consequently, an enhancement

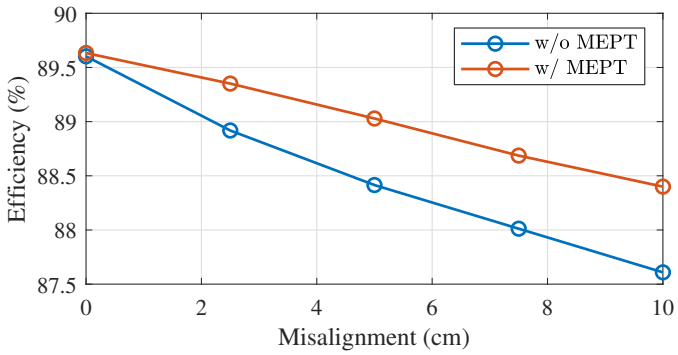

Figure 13. System efficiency depending on the horizontal misalignment of the coils, for operation with and without efficiency screening. For an output power of 3 kW.

of approximately 0.87 % is observed compared to operation with constant modulation when the system operates with active tracking.

VI. CONCLUSION

IPT charging represents a technology with significant potential to advance and solidify the electric vehicle industry. However, it still faces certain developmental constraints, particularly concerning the design and efficiency of the wireless transfer process. The methodology outlined in this article offers a means to optimize efficiency while ensuring that the system operates within predefined limits, particularly those related to system isolation (such as voltage in coils and capacitors) and maximum currents in semiconductors. As a result, manufacturers can tailor their component portfolios to better support the development of wireless chargers. The practical prototype demonstrated satisfactory functionality, meeting the specified limitations and delivering adequate performance in accordance with the SAE-J2954 standard. Furthermore, it was possible to verify the operation of a simple MEPT technique that guarantees better performance even with power variations and coil misalignment.

ACKNOWLEDGMENT

This work was financed in part by the Coordination for the Improvement of Higher Education Personnel – Brazil (CAPES/PROEX) – Finance Code 001. I thank INCT-GD and the Funding agencies (CNPq process 465640/2014-1, CAPES process no. 23038.000776/2017-54 and FAPERGS 17/2551-0000517-1) for the financial support.

VII. AUTHOR CONTRIBUTIONS

VIEIRA, L.A.B.: Conceptualization, Data Curation, Formal Analysis, Investigation, Methodology, Project Administration, Software, Validation, Visualization, Writing – Original Draft, Writing – Review & Editing. **PASCAL, P.**: Data Curation, Formal Analysis, Investigation, Methodology, Software, Validation, Visualization, Writing – Review & Editing. **RECH, C.**: Data Curation, Formal Analysis, Funding

Acquisition, Project Administration, Resources, Supervision, Visualization, Writing – Review & Editing.

PLAGIARISM POLICY

This article was submitted to the similarity system provided by Crossref and powered by iThenticate – Similarity Check.

References

[1] IEA, *World Energy Outlook 2021*, international energy agency, https://www.iea.org/reports/world-energy-outlook-2021.,, 2021.

[2] ABVE, *Eletrificados batem todas as previsões em 2021*, ASSOCIAÇÃO BRASILEIRA DE VEÍCULOS ELETRICOS, https://www.abve.org.br/eletrificados-batem-todas-as-previsoes-em-2021/, acesso 05/2022, 2022.

[3] H. H. Wu, A. Gilchrist, K. D. Sealy, D. Bronson, "A High Efficiency 5 kW Inductive Charger for EVs Using Dual Side Control", *IEEE Transactions on Industrial Informatics*, vol. 8, no. 3, pp. 585–595, 2012, doi:10.1109/TII.2012.2192283.

[4] D. J. Thrimawithana, U. K. Madawala, "A primary side controller for inductive power transfer systems", *in 2010 IEEE International Conference on Industrial Technology*, pp. 661–666, 2010, doi:10.1109/ICIT.2010.5472724.

[5] F. Grazian, W. Shi, T. B. Soeiro, J. Dong, P. Bauer, "Electric Vehicle Charging Based on Inductive Power Transfer Employing Variable Compensation Capacitance for Optimum Load Matching", *in IECON 2020 The 46th Annual Conference of the IEEE Industrial Electronics Society*, pp. 5262–5267, 2020, doi:10.1109/IECON43393.2020.9254920.

[6] S. Li, C. C. Mi, "Wireless Power Transfer for Electric Vehicle Applications", *IEEE Journal of Emerging and Selected Topics in Power Electronics*, vol. 3, no. 1, pp. 4–17, 2015, doi:10.1109/JESTPE.2014.2319453.

[7] X. Dai, X. Li, Y. Li, A. P. Hu, "Maximum Efficiency Tracking for Wireless Power Transfer Systems With Dynamic Coupling Coefficient Estimation", *IEEE Transactions on Power Electronics*, vol. 33, no. 6, pp. 5005–5015, 2018, doi:10.1109/TPEL.2017.2729083.

[8] A. Mahesh, B. Chokkalingam, L. Mihet-Popa, "Inductive Wireless Power Transfer Charging for Electric Vehicles–A Review", *IEEE Access*, vol. 9, pp. 137667–137713, 2021, doi:10.1109/ACCESS.2021.3116678.

[9] "SAE J2954: Wireless Power Transfer for Light-Duty Plug-In/Electric Vehicles and Alignment Methodology", , October 2020.

[10] X. Mou, O. Groling, A. Gallant, H. Sun, "Energy Efficient and Adaptive Design for Wireless Power Transfer in Electric Vehicles", *in 2016 IEEE 83rd Vehicular Technology Conference (VTC Spring)*, pp. 1–5, 2016, doi:10.1109/VTCSpring.2016.7504220.

[11] A. A. S. Mohamed, S. An, O. Mohammed, "Coil Design Optimization of Power Pad in IPT System for Electric Vehicle Applications", *IEEE Transactions on Magnetics*, vol. 54, no. 4, pp. 1–5, 2018, doi:10.1109/TMAG.2017.2784381.

[12] K. Aditya, V. K. Sood, "Design of 3.3 kW wireless battery charger for electric vehicle application considering bifurcation", *in 2017 IEEE Electrical Power and Energy Conference (EPEC)*, pp. 1–6, 2017, doi:10.1109/EPEC.2017.8286140.

[13] Z. Huang, T. Guan, Z. Wang, J. Wei, S. Wang, M. Liu, D. Sun, X. Zeng, "Maximum efficiency tracking design of wireless power transmission system based on machine learning", *Energy Reports*, vol. 8, pp. 447–455, 2022, doi:https://doi.org/10.1016/j.egyr.2022.10.139, 2022 The 5th International Conference on Renewable Energy and Environment Engineering.

[14] H. Li, J. Li, K. Wang, W. Chen, X. Yang, "A Maximum Efficiency Point Tracking Control Scheme for Wireless Power Transfer Systems Using Magnetic Resonant Coupling", *IEEE Transactions on Power Electronics*, vol. 30, no. 7, pp. 3998–4008, 2015, doi:10.1109/TPEL.2014.2349534.

[15] W. X. Zhong, S. Y. R. Hui, "Maximum Energy Efficiency Tracking for Wireless Power Transfer Systems", *IEEE Transactions on Power Electronics*, vol. 30, no. 7, pp. 4025–4034, 2015, doi:10.1109/TPEL.2014.2351496.

[16] T. Duerbaum, "First harmonic approximation including design constraints", *in INTELEC - Twentieth International Telecommunications Energy Conference (Cat. No.98CH36263)*, pp. 321–328, 1998, doi:10.1109/INTLEC.1998.793519.

[17] K. Aditya, S. S. Williamson, "Comparative study on primary side control strategies for series-series compensated inductive power transfer system", *in 2016 IEEE 25th International Symposium on Industrial Electronics (ISIE)*, pp. 811–816, 2016, doi:10.1109/ISIE.2016.7744994.

[18] I. Barbi, *Conversores CC-CC Básicos Não-Isolados*, Edição dos Autores, Florianopolis, Santa Catarina, 2006.

[19] A. K. Rathore, V. R. Vakacharla, "A Simple Technique for Fundamental Harmonic Approximation Analysis in Parallel and Series–Parallel Resonant Converters", *IEEE Transactions on Industrial Electronics*, vol. 67, no. 11, pp. 9963–9968, 2020, doi:10.1109/TIE.2019.2952820.

[20] W. Zhang, C. C. Mi, "Compensation Topologies of High-Power Wireless Power Transfer Systems", *IEEE Transactions on Vehicular Technology*, vol. 65, no. 6, pp. 4768–4778, 2016, doi:10.1109/TVT.2015.2454292.

[21] M. Zamani, M. Nagrial, J. Rizk, A. Hellany, "A review of inductive power transfer for electric vehicles", *in 2019 International Conference on Electrical Engineering Research Practice (ICEERP)*, pp. 1–5, 2019.

[22] A. Alphones, P. Jayathurathnage, "Review on wireless power transfer technology (invited paper)", *in 2017 IEEE Asia Pacific Microwave Conference (APMC)*, pp. 326–329, 2017.

[23] C. Nataraj, S. Khan, M. Habaebi, A. Muthalif, "Analysis of mutual inductance and coupling factor of inductively coupled coils for Wireless electricity", *ARPN Journal of Engineering and Applied Sciences*, vol. 12, pp. 4007–4012, 07 2017.

[24] A. Iyer, C. Bharatiraja, I. Vaghasia, V. Rajesh, "Design Optimisation for an Efficient Wireless Power Transfer System for Electric Vehicles", *Energy Procedia*, vol. 117, pp. 1015–1023, 06 2017.

[25] K. Aditya, V. K. Sood, S. Williamson, "Magnetic Characterization of Unsymmetrical Coil Pairs Using Archimedean Spirals for Wider Misalignment Tolerance in IPT Systems", *IEEE Transactions on Transportation Electrification*, vol. PP, no. 99, pp. 1–1, 2019, doi:10.1109/TTE.2019.2943321.

[26] P. G. Pascoal, "Projeto do acoplamento indutivo de um sistema de transferência de energia sem fio para a recarga de veículos elétricos", Trabalho de Conclusão de Curso (Graduação) — Universidade Federal de Santa Maria, Santa Maria, Brasil, Mar. 2023, URL: http://repositorio.ufsm.br/handle/1/28493.

[27] "IEC 60317-2: Specifications for particular types of winding wires - Part 2: Solderable polyurethane enamelled round copper wire, class 155", Edition 6.0, 2021.

[28] S. of Automotive Engineers (SAE), "Wireless Power Transfer for Light-Duty Plug-in Electric Vehicles and Alignment Methodology SAEJ2954", *SAE*, 2010.

[29] K. Aditya, V. K. Sood, "Design of 3.3 kW wireless battery charger for electric vehicle application considering bifurcation", *in 2017 IEEE Electrical Power and Energy Conference (EPEC)*, pp. 1–6, 2017, doi:10.1109/EPEC.2017.8286140.

[30] O. Stielau, G. Covic, "Design of loosely coupled inductive power transfer systems", *in PowerCon 2000. 2000 International Conference on Power System Technology. Proceedings (Cat. No.00EX409)*, vol. 1, pp. 85–90 vol.1, 2000, doi:10.1109/ICPST.2000.900036.

[31] J. Kennedy, R. Eberhart, "Particle swarm optimization", *in Proceedings of ICNN'95 - International Conference on Neural Networks*, vol. 4, pp. 1942–1948 vol.4, 1995, doi:10.1109/ICNN.1995.488968.

BIOGRAPHIES

Leonardo A. Brum Viera received his B.S. degree in Electrical Engineering from the Regional University of the Northwest of the State of Rio Grande do Sul (UNIJUÍ), Ijuí, Brazil, in 2019, and his M.S. degree in Electrical Engineering from the Federal University of Santa Maria (UFSM), Santa Maria, Brazil, in 2022. He is currently a Ph.D. student at the same university. From 2015 to 2019, he worked as a junior researcher at the Industrial Automation and Control Group, GAIC/UNIJUÍ. Since 2019, he has been a researcher at the Power Electronics and Control Group, GEPOC/INRI/UFSM, where

he conducts research in the field of electric vehicles, focusing on vehicle traction inverters and wireless charging systems. He currently serves as the president of the IEEE UFSM student branch.

Pedro Gelati Pascoal received the B.S. degree in electrical engineering from the Regional University of the Northwest of the State of Rio Grande do Sul (UNIJUÍ), Ijuí, Brazil, in 2020, and the M.S. degree in electrical engineering from the Federal University of Santa Maria (UFSM), Santa Maria, Brazil, in 2023. From 2016 to 2020, he was a junior researcher at the Industrial Automation and Control Group, GAIC/UNIJUÍ. From 2020 to 2023, he was a researcher at the Power Electronics and Control Group, GEPOC/INRI/UFSM. Since 2023, he has been a researcher at Centre for Power and Energy Systems (CPES/SGEVL) belonging to the Institute for Systems and Computer Engineering, Technology and Science (INESC TEC). His research interests include power electronics applied to electric vehicles charger systems.

Cassiano Rech (Senior Member, IEEE) received the B.S., M.S., and Ph.D. degrees in electrical engineering from the Federal University of Santa Maria (UFSM), Santa Maria, Brazil, in 1999, 2001, and 2005, respectively. From 2005 to 2007, he was with the Universidade Regional do Noroeste do Estado do Rio Grande do Sul, Ijuí, Brazil. From 2008 to 2009, he was with the Santa Catarina State University, Florianópolis, Brazil. Since 2009, he has been with the UFSM, where he is currently a Professor and Member of the Power Electronics and Control Research Group, GEPOC. Dr. Rech was Editor-in-Chief of the Brazilian Power Electronics Journal in 2014–2015. From 2016 to 2017, he was President of the Brazilian Power Electronics Society. Since 2018, he has been an Associate Editor for IEEE Transactions on Industrial Electronics. His research interests include multilevel converters, distributed energy resources, and power electronics applied to transportation electrification.